Integral Sliding Mode Control Design for Inverted Pendulum System Actuated by a Stepper Motor

Hiep Dai Le[1] and Tamara Nestorović[2]

***Abstract*— Although balancing of inverted pendulum is a well established problem, it continues to present more challenges in modern control designs. While sliding mode control has achieved considerable success in controlling inverted pendulums, most of these advancements have been primarily validated through simulations. Unfortunately, the complexity, and high computational demands of these controllers often limit practical implementation. To address these issues, we constructed a new inverted pendulum system, incorporating a stepper motor to reduce the backlash phenomenon commonly associated with a DC motor, thereby ensuring precise motion control. A simplified sliding mode controller was then designed for the augmented model of inverted pendulum and compared to a linear quadratic controller in practical implementation. The experimental results reveal that the sliding mode control significantly improves the system response, and effectively reduces the steady state errors in pendulum angle and cart position.**

I. INTRODUCTION

The cart inverted pendulum (CIP) is a common laboratory apparatus that is widely employed in human gait analysis, mobile robot balancing, and Segway [1]. In a typical CIP, the cart is driven backward and forward by a DC motor, while the pendulum freely rotates around a pivot point located at the top of the cart. The inverted pendulum system exhibits linear behaviour when the pendulum remains in the vicinity of the upright equilibrium position, but it exhibits strong nonlinear properties when the pendulum deviates significantly from that position. These characteristics make CIP a valuable tool for evaluating linear and nonlinear controllers [2]. Despite the simplicity of CIP designs, its control design poses challenges due to following reasons: 1) it is difficult to obtain an accurate model of practical systems that usually contain disturbances and uncertainties; 2) the nonminimum phase zero dynamics, coupling and other properties complicate the control design of CIP [3]. Therefore, addressing open problems such as internal coupling processes, transient performance improvement, complex dynamics analysis, and robustness enhancement has garnered more attention. Currently, various algorithms have been developed for CIP such as using Lyapunov theory [4], energy-based control [5], and feedback linearization [6]. While these controllers exhibit promising results in simulation studies, their real-time implementation often encounters limitations due to 1) the unavoidable disturbances and uncertainties in real systems, which can degrade control performance of CIP; 2) high computational cost and numerous tuning parameters, which hinder their practicality. One widely employed approach to solve disturbances and uncertainties is the sliding mode controller (SMC) [7]. SMC has obtained significant achievements in the design of fully actuated systems. However, these controllers face some challenges [8] in selecting proper sliding surfaces to stabilize both actuated and underactuated subsystems in the presence of strong internal coupling [9]. To address this problem, a coupled sliding mode control is designed for CIP. This approach includes a coupled linear sliding surface that integrates multiple independent state variables [10], ensuring the convergence of system states when it stays on the sliding surfaces; however, this method may lead to unpredictable transient processes [10]. Another SMC approach employs a cascade normal form [8]; however, obtaining this form can be challenging or may fail to meet some assumptions [11]. Several other approaches have been proposed for designing sliding surfaces of CIP including the regular form-based approach [12], linear matrix inequality (LMI) methods [13], and others. Among these, the regular form based approach [12] is widely used. This method involves applying a nonsingular coordinate transformation to convert the system model into a regular form, facilitating the design of sliding surface. To incorporate the advantages of linear quadratic regulator (LQR) control into sliding mode control, Utkin [12] successfully integrated the LQR approach into the sliding mode design in linear system models. However, the mathematical complexity of this approaches led Chen [14] to propose a new method for constructing the sliding surfaces, aiming at simplifying the design process. This approach enables the design of sliding surfaces to employ the pole assignment method in explicit form. Inspired by this, we propose a sliding mode control strategy for an augmented model of CIP to stabilize inverted pendulum at upright position. The control design is straight forward to implement and deliver high control performance. The remainder of this paper is organized as follows: Section II formulates the IP problem. Section III details the control design for the IP. Finally, Section IV demonstrates the simulation and experimental results.

II. PROBLEM FORMULATION

In our work, we present a new design of inverted pendulum system, as shown in Figure 1. The system consists of a pendulum mounted on a cart moving along a rail guide. Due to the limitations of employing a DC motor such as complexity related with gearbox utilization and imprecision caused

*This work was supported by DAAD (German Academic Exchange Service) and DFG (German Research Foundation) CRC-1683

[1] Hiep Dai Le is with Mechanics of Adaptive Systems, Ruhr-Universität Bochum, Germany Hiep.Le-d9b@ruhr-uni-bochum.de

[2] Tamara Nestorović is with Mechanics of Adaptive Systems, Ruhr-Universität Bochum, Germany tamara.nestorovic@rub.de

by backlash phenomenon, the stepper motor is employed to overcome these problems. This motor drives the cart along the straight rail guide via a belt while the pendulum freely rotates about the joint with horizontal axis located on the cart. $\theta(t)$ is the angular displacement of the pendulum with respect to the vertical upright position (rad); $\dot{\theta}(t)$ is the angular velocity of the pendulum (rad/s); $x(t)$ is the position of the cart (m); $\dot{x}(t)$ is the velocity of the cart (m/s); m_c is the cart mass (kg) and m_p is the pendulum mass (kg); L is the half-length of the pendulum (m); g is the acceleration of gravity (m/s^2); $u(t)$ is the required acceleration applied to the cart (m/s^2), representing in this case the control input.

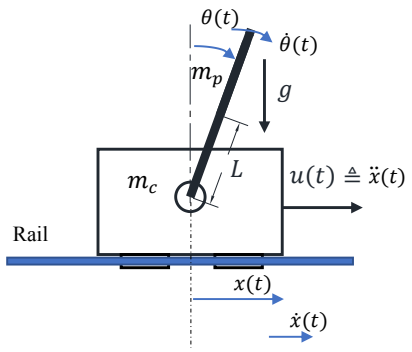

Fig. 1. CIP system driven by art acceleration via stepper motor

To eliminate the steady state errors of the cart position, an augmented model, which incorporates an integral cart position, is constructed for the control design [15]. The augmented model designed for our CIP system is given as [16]:

$$\dot{\mathbf{x}}_g(t) \triangleq \mathbf{A}_g \mathbf{x}_g(t) + \mathbf{b}_g u(t), \tag{1}$$

where

$$\mathbf{x}_g(t) \triangleq \begin{bmatrix} x(t) \\ \dot{x}(t) \\ \theta(t) \\ \dot{\theta}(t) \\ \int x(t) \end{bmatrix}; \tag{2}$$

$$\mathbf{A}_g \triangleq \begin{bmatrix} 0 & 1 & 0 & 0 & 0 \\ 0 & 0 & 0 & 0 & 0 \\ 0 & 0 & 0 & 1 & 0 \\ 0 & 0 & \frac{Lgm_p}{(m_pL^2+I)} & -\frac{k_d}{(m_pL^2+I)} & 0 \\ 1 & 0 & 0 & 0 & 0 \end{bmatrix}; \tag{3}$$

$$\mathbf{b}_g \triangleq \begin{bmatrix} 0 \\ 1 \\ 0 \\ -\frac{Lm_p}{(m_pL^2+I)} \\ 0 \end{bmatrix}. \tag{4}$$

In practical CIP systems, the uncertainties stemming from inaccurate modelling and external disturbances such as surrounding air flow, resistance, frictions etc. are unavoidable. The total value of uncertainties and external disturbances is defined as a lumped disturbance $\mathbf{d}(t) \in \mathbb{R}^{5\times 1}$, assumed to be unknown but bounded. Therefore, the practical CIP model (1) can be represented by

$$\dot{\mathbf{x}}_g(t) \triangleq \mathbf{A}_g \mathbf{x}_g(t) + \mathbf{b}_g u(t) + \mathbf{d}(t). \tag{5}$$

The lumped disturbance $\mathbf{d}(t)$ can be projected into the column spaces of $\mathbf{b}_g$ and $\mathbf{b}_g^{\perp}$, allowing it to be decomposed into matched $d_m(t)$ and unmatched lumped disturbance $\mathbf{d}_u(t)$ as given in [17]:

$$\mathbf{d}(t) = \mathbf{b}_g d_m(t) + \mathbf{d}_u(t), \tag{6}$$

where $d_m(t) = \mathbf{b}_g^{-left}\mathbf{d}(t)$ and $\mathbf{d}_u(t) = \mathbf{b}_g^{\perp}\mathbf{b}_g^{\perp-left}\mathbf{d}(t)$. In this notation $(\cdot)^{-left}$ stands for the left inverse of a matrix, here in particular: $\mathbf{b}_g^{-left} = (\mathbf{b}_g^{\mathrm{T}}\mathbf{b}_g)^{-1}\mathbf{b}_g^{\mathrm{T}}$ and the columns of $\mathbf{b}_g^{\perp} \in \mathbb{R}^{5\times 4}$ span the null space of $\mathbf{b}_g^{\mathrm{T}}$, in compliance with the *Proposition 1* in [17]. Therefore, the mathematical model (5) of the CIP system can be rewritten in the following form:

$$\dot{\mathbf{x}}_g(t) = \mathbf{A}_g \mathbf{x}_g(t) + \mathbf{b}_g(u(t) + d_m(t)) + \mathbf{d}_u(t). \tag{7}$$

III. CONTROL DESIGN

To design the sliding mode control, the sliding surface is designed to determine the behaviour of the system states under sliding mode and the control law is derived to ensure the system states reach and stay on the sliding surface despite the effect of the lumped disturbance [18]. There are various types of sliding surface designs; however, a linear sliding surface [12] $s(\mathbf{e}_g) \in \mathbb{R}$ is preferred due to its simplicity and effectiveness in ensuring the convergence. It is widely employed in practical applications, aiming to design a robust controller with minimal computational cost. The linear sliding surface is designed as

$$s(t) \triangleq \mathbf{c}\mathbf{x}_g(t), \tag{8}$$

where $\mathbf{c} \in \mathbb{R}^{1\times 5}$ is a design vector that could be selected to satisfy required control performance. When the sliding mode is achieved, i.e. $s(t) = 0$ and $\dot{s}(t) = 0$, the motion of the system states in sliding mode could be explained by using equivalent control technique [18]. The equivalent control $u_{eq}(t)$ is obtained by solving $u(t)$ in the time derivative of the sliding surface $\dot{s}(t) \equiv 0$.

$$\dot{s}(t) = \mathbf{c}(\mathbf{A}_g \mathbf{x}_g(t) + \mathbf{b}_g(u(t) + d_m(t)) + \mathbf{d}_u(t)) \equiv 0,\ \forall\, t \geq t_s \tag{9}$$

$$u_{eq}(t) = -(\mathbf{c}\mathbf{b}_g)^{-1}\mathbf{c}\left(\mathbf{A}_g \mathbf{e}_g + \mathbf{b}_g d_m(t) + \mathbf{d}_u(t)\right). \tag{10}$$

The sliding mode dynamic is determined by substituting (10) for $u(t)$ into (7)

$$\dot{\mathbf{x}}_g(t) = \left(\mathbf{I} - \mathbf{b}_g(\mathbf{c}\mathbf{b}_g)^{-1}\mathbf{c}\right)\mathbf{A}_g \mathbf{x}_g(t) + \left(\mathbf{I} - \mathbf{b}_g(\mathbf{c}\mathbf{b}_g)^{-1}\mathbf{c}\right)\mathbf{d}_u(t), \quad \forall\, t \geq t_s. \tag{11}$$

Define $\mathbf{k} \triangleq \mathbf{c}\mathbf{A}_g \in \mathbb{R}^{1\times 5}$, the sliding mode dynamic (11) can be simplified as follows

$$\dot{\mathbf{x}}_g(t) = (\mathbf{A}_g - \mathbf{b}_g\mathbf{k})\,\mathbf{x}_g(t) + \left(\mathbf{I} - \mathbf{b}_g(\mathbf{c}\mathbf{b}_g)^{-1}\mathbf{c}\right)\mathbf{d}_u(t), \tag{12}$$

It can be observed that the sliding mode dynamic (12) does not contain the matched disturbance, highlighting the properties of SMC in rejecting matched disturbances. However, unmatched disturbances are multiplied by $\mathbf{\Gamma} \triangleq (\mathbf{I} - \mathbf{b}_g(\mathbf{c}\mathbf{b}_g)^{-1}\mathbf{c})$. Furthermore, the sliding mode dynamics is independent of the control input, but depends on the selection of the value $\mathbf{c}$ of sliding surface $s(t)$. Since the values of $\mathbf{c}$ significantly affect the performance of sliding mode dynamics, selecting $\mathbf{c}$ should be careful to avoid amplifying unmatched disturbances. Motivated by [19], the value of $\mathbf{c}$ is determined by solving the following equation

$$\mathbf{c} = [\mathbf{k}\ \mathbf{I}][\mathbf{A}_g\ \mathbf{b}_g]^+, \tag{13}$$

where $[\mathbf{A}_g\ \mathbf{b}_g]^+$ is pseudo inverse, $\mathbf{k}$ can be found by LQR method, as in [15]

$$\mathbf{k} = \mathbf{R}^{-1}\mathbf{b}_g^{\mathrm{T}}\mathbf{P}, \tag{14}$$

where $\mathbf{P}$ is solved from algebraic Riccati equation (ARE)

$$\mathbf{A}_g^{\mathrm{T}} + \mathbf{P}\mathbf{A}_g + \mathbf{Q} - \mathbf{P}\mathbf{b}_g\mathbf{R}^{-1}\mathbf{b}_g^{\mathrm{T}}\mathbf{P} = 0, \tag{15}$$

where $\mathbf{Q}$ represents the state weighting matrix and $\mathbf{R}$ is the control weighting matrix. When the model parameters $\mathbf{A}_g$ and $\mathbf{b}_g$ are known, the ARE can be solved using a variety of techniques [20]. To drive the system states to the sliding surface (8), the reaching law is designed as in [21] in order to mitigate the chattering problem:

$$\dot{s}(t) = -k_{sw}|s(t)|^{\alpha}\mathrm{sgn}(s(t)),\ 0 < \alpha < 1, \tag{16}$$

where k_{sw} is a positive design parameter, and

$$\mathrm{sgn}(s(t)) = \begin{cases} 1 & \text{if } s(t) > 0, \\ 0 & \text{if } s(t) = 0, \\ -1 & \text{if } s(t) < 0. \end{cases}$$

As shown in (16), the reaching speed is adjusted based on the distance of the system states from the sliding surface. When the system states are far from the sliding surface, the reaching speed increases. Conversely, when the system states approach the sliding surface, the reaching speed decreases, mitigating the overshoot and chattering of control input.The term $|s(t)|^{\alpha}$ plays an important role in mitigating the chattering problem. However, selecting the value of α involves a trade-off: higher values improve chattering reduction, but they may compromise the robustness of the controller. The proposed control based on the reaching law (16) derived for system (7) using sliding surface (8) is:

$$u(t) \triangleq -(\mathbf{c}\mathbf{b}_g)^{-1}(\mathbf{c}\mathbf{A}_g\mathbf{x}_g(t) + k_{sw}|s(t)|^{\alpha}\mathrm{sgn}(s(t))). \tag{17}$$

The time derivative of the Lyapunov function $V \triangleq s^2/2$ is:

$$\dot{V}(t) = s(t)\dot{s}(t). \tag{18}$$

Substituting control input (17) into the time derivative of $s(t)$ (9) yields:

$$\dot{s}(t) = -k_{sw}|s(t)|^{\alpha}\mathrm{sgn}(s(t)) + d_m(t) + \mathbf{c}\mathbf{d}_u(t). \tag{19}$$

Therefore,

$$\dot{V}(t) = -k_{sw}|s(t)|^{\alpha+1}) + s(d_m(t) + \mathbf{c}\mathbf{d}_u(t)). \tag{20}$$

TABLE I

PARAMETERS SETTING FOR THE COMPARED CONTROLLERS

Controller	Tuning parameters			
ILQR	$R = 1$	$\mathbf{Q} = 0.01diag(1\ 0.1\ 5\ 0.2\ 10)$		
Present	$R = 1$	$\mathbf{Q} = 0.01diag(1\ 0.1\ 5\ 0.2\ 10)$	$k_{sw} = 1$	$\alpha = 0.7$

Selecting $k_{sw} \geq |(d_m + \mathbf{c}\mathbf{d}_u)/s^{\alpha}|$, we will have $\dot{V}(t) \leq 0$, $s \to 0$.

IV. EXPERIMENTAL RESULTS

The effectiveness of the proposed control is verified by experimental studies, carried out on a CIP prototype, developed at Department *Mechanics of Adaptive Systems*, Ruhr-Universtät Bochum, shown in Figure 2. A stepper motor Sanyo Denki 103h7123-5040 is used to exert the cart acceleration determined by the proposed controller. The pendulum angle is measured by the rotary magnetic encoder module RMB28AC with a resolution of 1024 counts/rev installed at the end of the pendulum. A miniature incremental magnetic encoder module RLC2HD with a resolution of 80000 counts/m is employed to measure the cart position along the magnetic scale. Both encoder signals are transmitted to dSPACE Scalexio with a sampling time of 0.001 s. The acceleration exerted on the cart, calculated by the proposed controller, is converted into pulse width modulated (PWM) signal and provided to a microstep driver of the stepper motor via dSPACE Scalexio. The physical parameters of our CIP model are given as follows: $g = 9.81$ m/s^2; the mass of the cart $m_c = 0.8$ kg; the mass of the pendulum $m_p = 0.188$ kg; the half-length of the pendulum $L = 0.34$ m . Several nuts are attached to the tip of the pendulum, considered as unknown lumped disturbance. The initial conditions of the CIP are set as $\mathbf{x}(t_0) = [0.036\ 0\ 0.124\ 0]^{\mathrm{T}}$ by adjusting the angle of the pendulum clamp and the cart position. The proposed control is compared with the integral linear quadratic regulator (ILQR) control [16] to evaluate its effectiveness. The control law of the ILQR designed for our CIP is [16]:

$$u_{\mathrm{ILQR}}(t) \triangleq -\mathbf{R}^{-1}\mathbf{b}_g^{\mathrm{T}}\mathbf{P}\mathbf{x}_g(t), \tag{21}$$

where $\mathbf{P}$ is a symmetric positive definite matrix obtained as the solution of the algebraic Riccati equation (15). The primary control parameters of ILQR [16] and the parameters of the controller proposed in this paper are listed in Table I. In order to verify the effectiveness of the proposed control, experimental stabilization results of the CIP are presented in this section, which detail the data available at this **link**. Note that the swing-up process is not utilized in these experiment, and the initial conditions of the CIP are set manually.

Fig. 3 and Fig. 4 compare the control performance of the ILQR and the proposed controller regarded to the cart position and the pendulum angle, respectively. Both controllers successfully balance the CIP from the small initial pendulum angle $\theta_0 = 0.124$ rad; however the cart position plots in Fig. 3 reveal notable differences in their performance. While the ILQR produces substantial cart position errors of approximately 0.26 m at the beginning of the response,

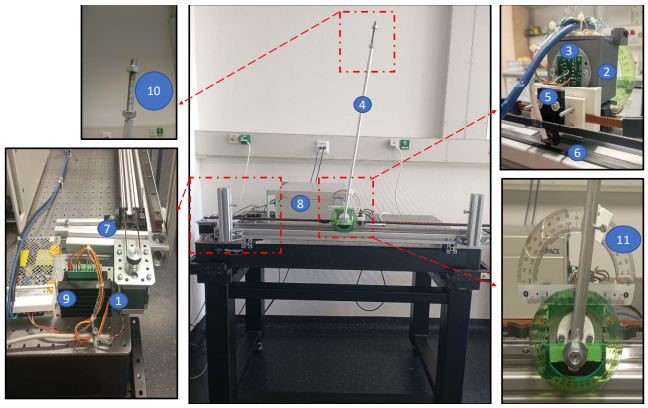

Fig. 2. Parts of the experimental rig with CIP: 1) stepper motor; 2) cart; 3) rotary magnetic encoder module pendulum clamp; 4) pendulum; 5) miniature incremental magnetic encoder module; 6) magnetic scale; 7) belt; 8) dSPACE; 9) microstep driver; 10) nuts; 11) pendulum clamp.

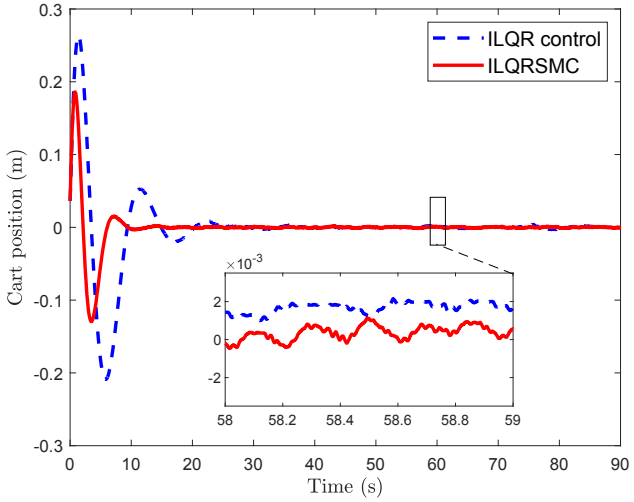

Fig. 3. Cart position of stabilization problem

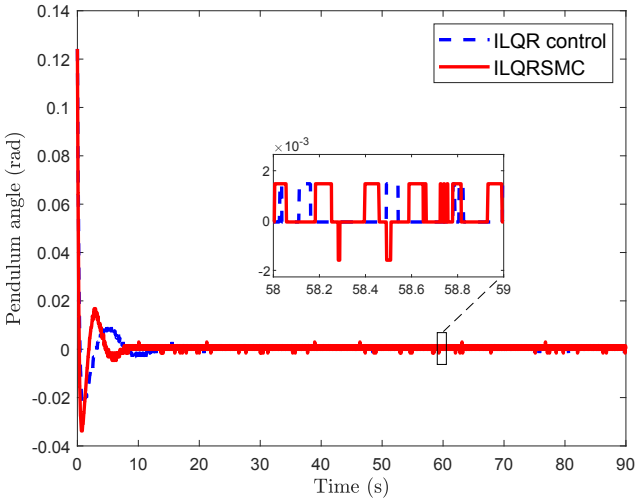

Fig. 4. Pendulum angle of stabilization problem

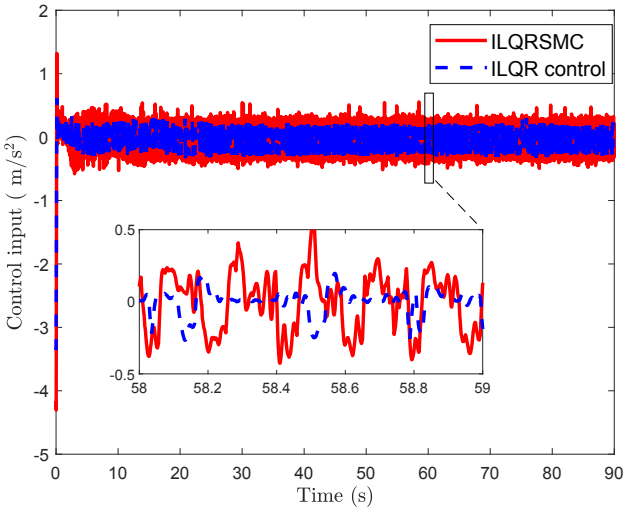

Fig. 5. Control input of stabilization problem

the proposed controller achieves smaller errors and reduced oscillation, decreasing the initial errors by about 30%. After 25 s, ILQR achieves satisfactory performance, whereas it only takes approximately 10 s for the proposed controller to reach a similar level of performance. Although the steady state tracking errors of the cart position in both controllers stay round 2×10^{-3} m, the peak overshoot of the cart position is substantially diminished from 0.26 m to 0.18 m in the proposed controller. From Fig. 4, both the ILQR and the proposed control perform rapid responses, bringing the pendulum from its initial error to its upright position within 10 s , and achieving a steady-state error within the range of $[-0.001 \;\; 0.001]$ rad. A detailed quantitative analysis is presented in Table II, providing the index values of the integrated absolute error (IAE) for both the cart position error and the pendulum angle error. These indexes are defined from [22]:

$$\mathrm{IAE}_x = \int_0^T |x(t) - x_d(t)| dt, \tag{22}$$

$$\mathrm{IAE}_\theta = \int_0^T |\theta(t) - \theta_d(t)| dt, \tag{23}$$

where T is the running time, IAE_x and IAE_θ are integrated absolute values of the cart position error and of the pendulum angle error, respectively. While smaller IAE values indicate better tracking performance as they reflect less accumulation of tracking errors, higher values of IAE imply a greater accumulation of tracking errors, causing poorer tracking capability. In this context, the proposed control exhibits an IAE_x index of 0.6233 m for cart position, while this index for ILQR is 1.6714 m. However, the proposed control reaches a slightly higher IAE_θ index value for pendulum angle at 0.1292 rad, which can be attributed to initial errors from 0-10 s. Although, the proposed control provides superior stabilization performance for the CIP, its control signal is higher than that of the ILQR controller, as shown in Fig. 5. To evaluate the required control energy of these controllers,

the integral absolute control (IAC) index is used, defined as [23]

$$\text{IAC} = \int_0^T |u(t)|dt. \tag{24}$$

The IAC values demonstrate the control effort, where smaller values indicate more energy efficient control. The proposed control requires higher a control effort compared to ILQR control, as exhibited by an IAC index of 16.06. This high control effort stems from the reaching law, which is designed to compensate the matched disturbances. The parameter α in the power reaching law (16) governs a trade off between tracking accuracy and control smoothness. Small values of α improve convergence speed and tracking accuracy of system states, but significantly increase control effort due to intensified chattering. When the value of α is too small such as $\alpha = 0.3$, the chattering in control input becomes excessive, potentially degrading the overall control accuracy, as given in Table III. To verify the robustness of proposed controller, matched disturbances are introduced to the CIP system. A step disturbance of $d_m = 0.08$ m/s^2 is applied for CIP system between 30 and 50 s, followed by a sinusoidal disturbance of $d_m = 0.08\sin(0.1t)$ m/s^2 between 70 and 90 s. The corresponding results are given in Fig. 6 - Fig.8, demonstrating the superior performance of the proposed control compared to ILQR in terms of disturbance rejection capabilities. Under both types of disturbances, it drives the cart position and pendulum angle to desired values more quickly compared to ILQR control, whereas ILQR's performance significantly deteriorates. When step disturbance is applied at t =30 s, ILQR control generates a large overshoot of 0.07 m in cart position, followed by an undershoot of -0.06 m after the disturbance is removed at t =50 s. This highlights ILQR's sensitivity to disturbances. Similarly, under sinusoidal disturbances, ILQR generates high tracking errors, whereas the proposed control demonstrates small tracking errors, showing its superior disturbance rejection.

TABLE II

INDEX VALUES OF CONTROL STRATEGIES IN STABILIZATION CONTROL

Controller	IAE of **cart position** (m)	IAE of **pendulum angle** (rad)	IAC
ILQR	1.6714	0.1209	7.8814
Present	0.6233	0.1292	16.0692

TABLE III

INFLUENCE α VALUES IN CONTROL PERFORMANCE

Presented control	IAE of **cart position** (m)	IAE of **pendulum angle** (rad)	IAC
$\alpha = 0.3$	0.5855	0.3160	74.5306
$\alpha = 0.5$	0.5763	0.1793	32.07
$\alpha = 0.9$	0.6982	0.1060	9.48

V. CONCLUSIONS

This paper presents results of a novel approach to practical implementation of the controller for stabilization of the cart with inverted pendulum (CIP) system. The controller

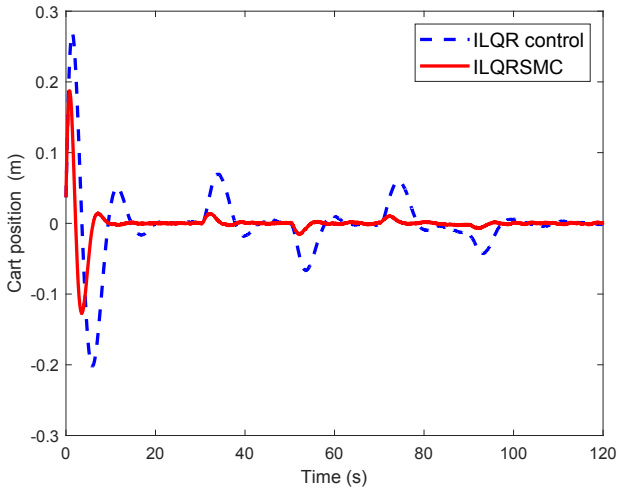

Fig. 6. Cart position of stabilization problem in presence of disturbances

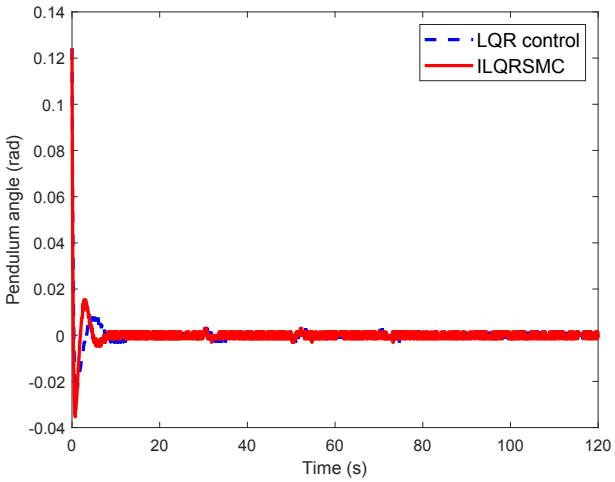

Fig. 7. Pendulum angle of stabilization problem in presence of disturbances

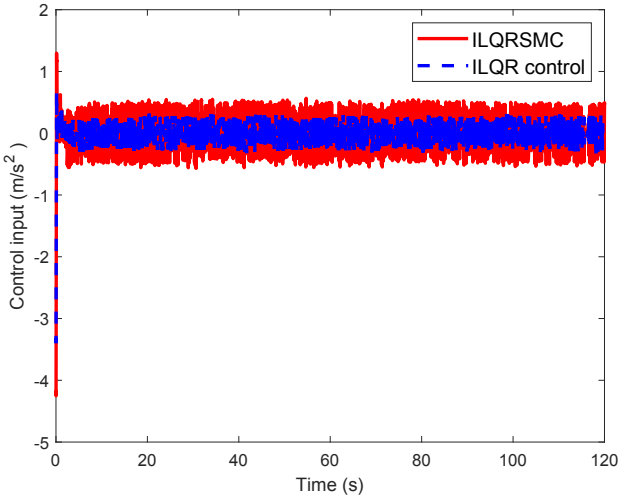

Fig. 8. Control input of stabilization problem in presence of disturbances

is based on sliding mode control (SMC) incorporating the SMC properties which enable to account for the presence of unknown lumped disturbances in the system. In the experimental setup they are modelled by adding weights to the pendulum mass. The controller is compared with the integral LQR controller (ILQR) proposed earlier by the authors for the CIP stabilization. The experimental investigations have shown that the present controller exhibits superiority in the overall performance compared to the previous state of the art.

REFERENCES

[1] Olfa Boubaker. The inverted pendulum: A fundamental benchmark in control theory and robotics. In *International conference on education and e-learning innovations*, pages 1–6. IEEE, 2012.

[2] Lubaid Nisar, Majid Hameed Koul, and Babar Ahmad. Controller design aimed at achieving the desired states in a 2-dof rotary inverted pendulum. *IFAC-PapersOnLine*, 57:256–261, 2024.

[3] Mark W Spong. Underactuated mechanical systems. In *Control problems in robotics and automation*, pages 135–150. Springer, 2005.

[4] Carlos Aguilar Ibanez, O Gutierrez Frias, and M Suarez Castanon. Lyapunov-based controller for the inverted pendulum cart system. *Nonlinear Dynamics*, 40:367–374, 2005.

[5] Mark W Spong. Energy based control of a class of underactuated mechanical systems. *IFAC Proceedings Volumes*, 29(1):2828–2832, 1996.

[6] Carlos Aguilar Ibanez and O Gutierrez Frias. Controlling the inverted pendulum by means of a nested saturation function. *Nonlinear Dynamics*, 53:273–280, 2008.

[7] Vadim Utkin. Variable structure systems with sliding modes. *IEEE Transactions on Automatic control*, 22(2):212–222, 1977.

[8] Reza Olfati-Saber. *Nonlinear control of underactuated mechanical systems with application to robotics and aerospace vehicles*. PhD thesis, Massachusetts Institute of Technology, 2001.

[9] Biao Lu, Yongchun Fang, and Ning Sun. Continuous sliding mode control strategy for a class of nonlinear underactuated systems. *IEEE Transactions on Automatic Control*, 63(10):3471–3478, 2018.

[10] Mun-Soo Park and Dongkyoung Chwa. Swing-up and stabilization control of inverted-pendulum systems via coupled sliding-mode control method. *IEEE transactions on industrial electronics*, 56(9):3541–3555, 2009.

[11] Rong Xu and Ümit Özgüner. Sliding mode control of a class of underactuated systems. *Automatica*, 44(1):233–241, 2008.

[12] VI Utkin. Methods for constructing discontinous planes in multidimensional variable structure systems. *Automation and Remote control*, 31:1466–1470, 1977.

[13] Christopher Edwards. A practical method for the design of sliding mode controllers using linear matrix inequalities. *Automatica*, 40(10):1761–1769, 2004.

[14] Yon-Ping Chen and Jeang-Lin Chang. A new method for constructing sliding surfaces of linear time-invariant systems. *International Journal of Systems Science*, 31(4):417–420, 2000.

[15] Hanmant G Malkapure and M Chidambaram. Comparison of two methods of incorporating an integral action in linear quadratic regulator. *IFAC Proceedings Volumes*, 47(1):55–61, 2014.

[16] Hiep Dai Le and Tamara Nestorović. Integral linear quadratic regulator for inverted pendulum system actuated by a step motor. In *2024 10th International Conference on Control, Decision and Information Technologies (CoDIT)*, pages 367–370. IEEE, 2024.

[17] Fernando Castanos and Leonid Fridman. Analysis and design of integral sliding manifolds for systems with unmatched perturbations. *IEEE Transactions on Automatic Control*, 51(5):853–858, 2006.

[18] Vadim I Utkin. *Sliding modes in control and optimization*. Springer Science & Business Media, 2013.

[19] Branislava Draženović, Čedomir Milosavljević, and Boban Veselić. Comprehensive approach to sliding mode design and analysis in linear systems. In *Advances in sliding mode control: concept, theory and implementation*, pages 1–19. Springer, 2013.

[20] Gary Hewer. An iterative technique for the computation of the steady state gains for the discrete optimal regulator. *IEEE Transactions on Automatic Control*, 16(4):382–384, 1971.

[21] Weibing Gao and James C Hung. Variable structure control of nonlinear systems: A new approach. *IEEE transactions on Industrial Electronics*, 40(1):45–55, 1993.

[22] Li Yu, Guang He, Xiangke Wang, and Shulong Zhao. Robust fixed-time sliding mode attitude control of tilt trirotor uav in helicopter mode. *IEEE Transactions on Industrial Electronics*, 69(10):10322–10332, 2021.

[23] Zwe-Lee Gaing. A particle swarm optimization approach for optimum design of pid controller in avr system. *IEEE transactions on energy conversion*, 19(2):384–391, 2004.